Make Space to Change Lane: A Cooperative Adaptive Cruise Control Lane Change Controller*

Haoran Wang, and Jia Hu, *Member, IEEE*

Abstract— **This research proposes a Cooperative Adaptive Cruise Control Lane Change (CACCLC) controller. It is designed for making space to change lane successfully. The proposed controller has the following features: i) capable of making space to change lane by adopting a new Backward-Looking (BL) information topology; ii) with string stability; iii) with consideration of vehicle dynamics. The proposed CACCLC controller is evaluated on a joint simulation platform consisting of PreScan and Matlab/Simulink. Results demonstrate that: i) a lane-change gap for a single vehicle could be utilized for CACCLC maneuver; ii) the proposed CACCLC controller is with string stability and could eliminate 66.76% gap error from the end to the start of a platoon. Moreover, the computation time of the proposed CACCLC controller is approximately 15 milliseconds when running on a laptop equipped with an Intel i7-8750H CPU. This indicates that the proposed controller is ready for real-time implementation.**

I. Introduction

Cooperative Adaptive Cruise Control (CACC) is a key technology among the applications of Connected Automated Vehicle (CAV). By enabling Adaptive Cruise Control (ACC) with communication and cooperation, CACC reduces platoon time headway to 0.5 seconds according to field tests, much smaller than the 1-2 seconds headway of Human-driven Vehicle (HV) [1-3]. This headway reduction benefits driving mobility by nearly doubling conventional road capability [4-7]. CACC is also forecasted to increase driving safety by over-the-horizon cooperation [8]. Moreover, CACC has been proven to yield 10-20% energy-saving [9] and reduce 14% carbon dioxide emission [10].

Conventional CACC controllers are mostly longitudinal only. However, when implemented in field, lateral lane-change capability is critical for a CACC platoon. Lack of Platoon Lane-Change (PLC) control may force the CACC system to disengage when PLC maneuver is unavoidable [11-13]. This platoon disengagement may: i) break the running continuity of CACC systems; ii) call for more unnecessary human take-overs; iii) impede traffic when looking for lane-change gaps [7].

However, only a few past studies make efforts on CACC Lane Change (CACCLC) controllers. Based on spline curve interpolation method, various CACCLC controllers are proposed [14, 15]. However, these controllers are without the consideration of vehicle dynamics. It may make control commands unfeasible for a vehicle to fulfill. To solve this problem, Huang proposed a artificial potential based CACCLC controller [16]. It considers vehicle dynamics in the optimal control problem formulation. However, this method may result in local optimum that casts risk on driving safety. Moreover, all these controllers are at risk of cutting off the platoon string. It not only decreases the success rate of lane-change, but also breaks the running continuity. For example, in the scenario as shown in Figure 3, conventional CACC systems still have to disengage since there is not a gap for the platoon to change lane simultaneously.

String stability of a CACC system is necessary for safeguarding against disturbance [17]. Various longitudinal only CACC controllers with string stability have been proposed. These controllers follow information topologies including predecessor following [18, 19], predecessor-leader following [20, 21], and bi-directional [22]. However, all past CACCLC controllers have not been proven with string stability.

Therefore, a next generation CACCLC controller is proposed in this paper to address inevitable needs for PLC maneuver. This new type CACCLC controller is with following features:

- With 100% success rate of lane-change;
- With consideration of vehicle dynamics;
- With string stability.

The remainder of this paper is organized as follows. Section II presents the research scope of this paper. Section III formulates the CACCLC controller and presents a solution algorithm. Section IV proves the string stability. Section V evaluates the proposed controller in simulation. Section VI makes a conclusion and provides future research ideas.

II. Research Scope

The goal of the proposed CACCLC controller is to make space for a CACC platoon to change lane with 100% success rate. There are three high lights of this controller:

- **Making space to change lane**: The proposed controller is capable of broadening the lane change gap for lane change maneuver. It not only lowers the threshold of CACCLC gap, but also ensures a 100%-success-rate CACCLC maneuver.
- **Based on vehicle dynamics**: The consideration of vehicle dynamics ensures the motion commands feasible for vehicle to fulfill.
- **String stable**: The proposed CACCLC controller is proved with string stability.

*Resrach supported by National Natural Science Foundation of China (Grant No. 61803284 & 61903058), Shanghai Oriental Scholar (2018), Shanghai Yangfan Program (No. 18YF1424200), Tongji Zhongte Chair Professor Foundation (No. 000000375-2018082), National Key R&D Program of China (No. 2018YFB1600600)

Haoran Wang and Jia Hu are with Key Laboratory of Road and Traffic Engineering of the Ministry of Education, Tongji University, Shanghai 201804, China (e-mail: 1314haoran@tongji.edu.cn; hujia@tongji.edu.cn)

Manuscript 497 submitted to 2021 32nd IEEE Intelligent Vehicles Symposium (IV).
Received April 7, 2021.

A. System Structure

The proposed CACCLC controller is adopted in the system illustrated in Figure 1. This system consists of three modules. The module 2 is discussed in this paper. Details of each module are provided as follows:

- Module 1: This module is in charge of lane-change gap selection. A gap enough for a single CAV to change lane could be utilized for CACCLC maneuver. State and position information of all CAVs in a platoon and surrounding vehicles are then collected.
- Module 2: Receiving information from module 1, this module plans trajectories by the proposed CACCLC controller. Control commands are then given to module 3.
- Module 3: This module actuates control commands provided by the proposed CACCLC controller.

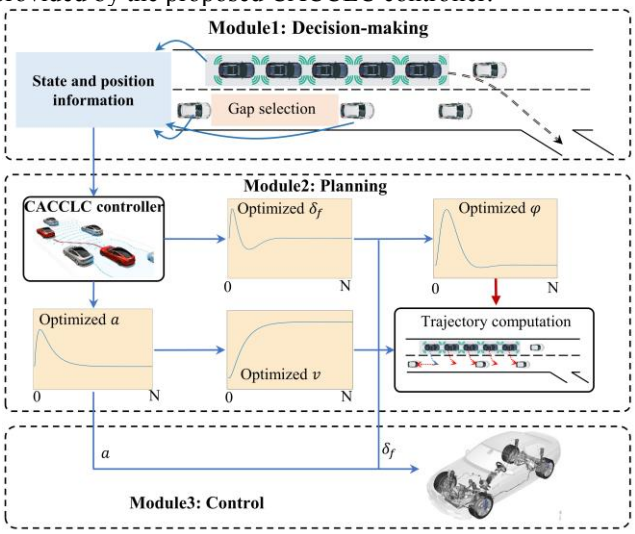

Figure 1. System structure

B. Control Logic

With the objective of making space for CACCLC, a new information flow topology, Backward-Looking (BL), is adopted as illustrated in Figure 2. In the BL topology, information is passed on from the rear CAV to its predecessor.

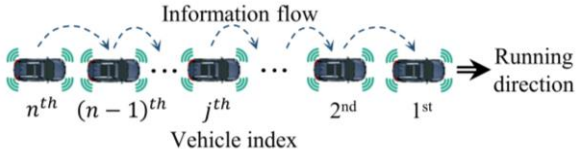

Figure 2. Backward-Looking information topology

Based on the BL topology, the control logic of the proposed controller is proposed in Figure 3. CACCLC maneuver is realized by the following tactics:

Step 1: Receiving the information of the selected gap, the front vehicle, and the rear vehicle.

Step 2: Maneuvering the last CAV to change lane.

Step 3: Slowing the last CAV to enlarge the gap.

Step 4: Maneuvering CAVs to change lane in turn from the last CAV to the first CAV.

Step 5: CACCLC maneuver pauses when a vehicle cuts in. This vehicle is selected as the new front vehicle. Then go back to the step 3.

Step 6: CACCLC maneuver is finished.

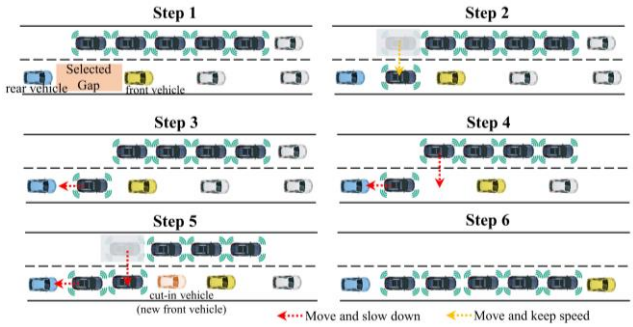

Figure 3. The control logic of the proposed CACCLC controller

C. Control Objective

To achieve the proposed CACCLC tactics, the control objective of the proposed motion planner is decomposed as follows:

- Longitudinal objective: Based on BL topology, each CAV follows the CAV behind it. Longitudinal objective of the proposed controller is to minimize the gap error. The gap error is defined as follows:

$$e_g^j(t) \stackrel{\text{def}}{=} \left| x^j(t) - x^{j+1}(t) - g_{des} \right| \tag{1}$$

where g_{des} is the desired space gap.

- Lateral objective: Lateral objective of the proposed controller is to minimize lateral position error. The lateral position error is defined as follows:

$$e_y^j(t) \stackrel{\text{def}}{=} \left| y^j(t) - y_{des}^j(t) \right| \tag{2}$$

where y_{des}^j is the lateral position of the current lane centerline. When the gap is enough for the jth vehicle to change lane in the Step 3, y_{des}^j is the lateral position of the desired lane centerline.

III. Problem Formulation

The proposed CACCLC controller is formulated in this section. It consists of a longitudinal controller and a lateral controller. The longitudinal controller is designed to minimize the gap error. The lateral controller is designed to minimize lateral position error. The two controllers together fulfill the ultimate goal: making space to change lane.

Figure 4 illustrates a typical scenario where a platoon must change lane before the ramp. Indices and parameters utilized in this paper are defined in TABLE I. Some of them are depicted in Figure 4 for better illustration purpose.

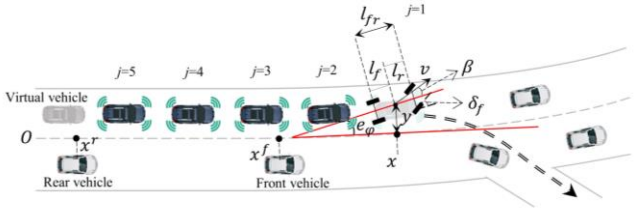

Manuscript 497 submitted to 2021 32nd IEEE Intelligent Vehicles Symposium (IV).
Received April 7, 2021.

Figure 4. Scenairo notations

TABLE I INDICES AND PARAMETERS

Indices	Definition
a	Acceleration (m/s^2)
a^j	Acceleration of the *j*th CAV in a platoon (m/s^2)
a_{min}	Minimum acceleration (m/s^2)
a_{max}	Maximum acceleration (m/s^2)
a^α	Acceleration of the virtual vehicle (m/s^2)
$\boldsymbol{A}_{x,n}$	State coefficient matrix in the longitudinal dynamics of a CACC system with n CAVs
$\boldsymbol{A}_{y,n}$	State coefficient matrix in the lateral dynamics of a CACC system with n CAVs
$\boldsymbol{B}_{x,n}$	Control coefficient matrix in the longitudinal dynamics of a CACC system with n CAVs
$\boldsymbol{B}_{y,n}$	Control coefficient matrix in the lateral dynamics of a CACC system with n CAVs
$\boldsymbol{C}_{x,n}$	Constant matrix in the longitudinal dynamics of a CACC system with n CAVs
$\boldsymbol{C}_{y,n}$	Constant matrix in the lateral dynamics of a CACC system with n CAVs
$\widetilde{\boldsymbol{D}}_i$	A concomitant matrix in the solution algorithm
e	The natural logarithm
$\bar{e}_g$	Mean of absolute gap error (meters)
e_g^j	Gap error of the *j*th CAV (meters)
e_y^j	Lateral position error of the *j*th CAV in a platoon (meters)
e_φ	Heading angle error (rad)
e_φ^j	Heading angle error of the *j*th CAV in a platoon (rad)
$\boldsymbol{E}_n$	A parameter matrix of the platoon control vector with n CAVs in frequency domain
f_x	Longitudinal system dynamics function
f_y	Lateral system dynamics function
$\boldsymbol{F}_n$	A parameter matrix of the platoon control vector with n CAVs in frequency domain
$g(x)$	A x-domain function
$G(s)$	The format of function $g(x)$ in frequency domain
g_{des}	Desired following gap (meters)
g_{min}	Safe following gap (meters)
g_{min}^{HV}	Safe following gap between CAV and HV (meters)
H	Hamiltonian function
i	Control step index
$\boldsymbol{I}$	Identity matrix
j	Vehicle index in a platoon
J_x	Longitudinal cost function
J_y	Lateral cost function
k	The index of surrounding vehicles
l_{fr}	Distance between front axle and rear axle (meters)
l_f	Distance between vehicle's gravity center and front axle (meters)
l_r	Distance between vehicle's gravity center and rear axle (meters)
L_x	Longitudinal running cost function
L_y	Lateral running cost function
$\mathcal{L}$	Laplace operator
M_x	Longitudinal terminal state cost
M_y	Lateral terminal state cost
$\boldsymbol{M}_n$	A parameter matrix of the platoon control vector with n CAVs in frequency domain
n	Number of CAVs in a platoon
N	Total control steps
$\mathbb{N}$	Natural numbers set
$\boldsymbol{O}_{n,j}$	A parameter matrix in the transfer function between the *j*th CAV and the virtual vehicle for a platoon with n CAVs
q_g	Weighting factor for gap error
q_v	Weighting factor for speed error
q_y	Weighting factor for lateral error
q_φ	Weighting factor for heading error
$\boldsymbol{Q}_{x,n}$	Longitudinal state weighting factor matrix for a CACC system with n CAVs
$\boldsymbol{Q}_{y,n}$	Longitudinal state weighting factor matrix for a CACC system with n CAVs
$\widetilde{\boldsymbol{Q}}_i$	A concomitant matrix in the solution algorithm
r_a	Weighting factor for acceleration efforts
r_δ	Weighting factor for steering efforts
$\boldsymbol{R}_{x,n}$	Longitudinal control weighting factor matrix for a CACC system with n CAVs
$\boldsymbol{R}_{y,n}$	Longitudinal control weighting factor matrix for a CACC system with n CAVs
$\mathbb{R}^+$	Positive set
$\boldsymbol{r}_n$	The co-state vector in the frequency domain for a CACC system with n CAVs
s	A complex variable
t	Global time (seconds)
$\boldsymbol{u}_{x,n}$	Longitudinal control vector for a CACC system with n CAVs
$\boldsymbol{u}_{y,n}$	Lateral control vector for a CACC system with n CAVs
$\boldsymbol{u}_{x,n}^*$	The optimal longitudinal control vector for a CACC system with n CAVs
$\boldsymbol{U}_n$	The control vector of a platoon with n CAVs in the frequency domain
v	Vehicle speed (*m/s*)
v^j	Speed of the *j*th CAV in a platoon (*m/s*)
v_{des}	Desired speed to make space for lane-change
v^α	Speed of the virtual vehicle (*m/s*)
x	Longitudinal position (meters)
x^f	Longitudinal position of the front vehicle (meters)
x^r	Longitudinal position of the rear vehicle (meters)
x^j	Longitudinal position of the *j*th CAV in a platoon (*m/s*)
x^α	Longitudinal position of the virtual vehicle
$\boldsymbol{X}_n$	The state vector of a platoon with n CAVs in the frequency domain
y	Vehicle lateral position (meters)
y_{max}	Maximum lateral position (meters)
y_{min}	Maximum lateral position (meters)
y^j	Lateral position of the *j*th CAV in a platoon (meters)
y_{des}^j	Lateral position of the desired lane centerline
$\boldsymbol{Z}_{1_i}$	A parameter matrix in concomitant matrices at step i
$\boldsymbol{Z}_{2_i}$	A parameter matrix in concomitant matrices at step i
$\boldsymbol{Z}_{3_i}$	A parameter matrix in concomitant matrices at step i
$\boldsymbol{Z}_{4_i}$	A parameter matrix in concomitant matrices at step i
$\boldsymbol{Z}_{5_i}$	A parameter matrix in concomitant matrices at step i
α	The index of the virtual vehicle
β	Vehicle slip angle (rad)
$\Theta_{n,j,j+1}$	Transfer function between CAV j and CAV $j+1$ in a platoon with n CAVs
$\Theta_{n,j,\alpha}$	Transfer function between CAV j and the virtual vehcilein a platoon with n CAVs
δ_f	Front wheel angle (rad)
δ_f^j	Front wheel angle of the *j*th CAV in a platoon (rad)
$\delta_{f\,min}$	Minimum front wheel angle (rad)
$\delta_{f\,max}$	Maximum front wheel angle (rad)
ι	Imaginary number
κ	Road curvature
$\boldsymbol{\lambda}_n$	The co-state vector for a platoon with n CAVs
$\boldsymbol{\lambda}_n^*$	The optimal co-state vector
$\boldsymbol{\mu}^j$	Control vector of the jth CAV in the frequency domain
$\boldsymbol{\xi}_{x,n}$	Longitudinal state vector for a CACC system with n CAVs
$\boldsymbol{\xi}_{x,n}^*$	The optimal longitudinal state vector for a CACC system with n CAVs
$\boldsymbol{\xi}_{y,n}$	Lateral state vector for a CACC system with n CAVs
τ	Control time step (seconds)
φ	Heading angle (rad)
ω	Angular speed in the Laplace domain

A. State Definition

State and control variables are defined in Definition 1. A virtual vehicle is first assumed in Assumption 1 to guide the last CAV to slow down for gap broadening.

Assumption 1: There is a virtual vehicle α with the following settings:

Manuscript 497 submitted to 2021 32nd IEEE Intelligent Vehicles Symposium (IV).
Received April 7, 2021.

$$v^{\alpha} \stackrel{\text{def}}{=} v_{des} \tag{3}$$
$$x^{\alpha}(0) \stackrel{\text{def}}{=} x^{n}(0) - g_{des} \tag{4}$$
$$a^{\alpha} \stackrel{\text{def}}{=} 0 \tag{5}$$
$$\frac{dx^{\alpha}}{dt} \stackrel{\text{def}}{=} v^{\alpha} \tag{6}$$

where v^{α} is the speed of the virtual vehicle; v_{des} is the desired speed to make space for lane-change; x^{α} is the longitudinal position of the virtual vehicle; a^{α} is the acceleration of the virtual vehicle; $x^{n}(0)$ is the initial longitudinal position of the last vehicle in a platoon.

Definition 1: For a CACC system with n CAVs, longitudinal state vector $\boldsymbol{\xi}_{x,n}$, longitudinal control vector $\boldsymbol{u}_{x,n}$, lateral state vector $\boldsymbol{\xi}_{y,n}$, and lateral control vector $\boldsymbol{u}_{y,n}$ are defined as follows:

$$\boldsymbol{\xi}_{x,n} \stackrel{\text{def}}{=} [v^{n} - v^{\alpha}, x^{n} - x^{\alpha} - g_{des}, \cdots, v^{j} - v^{j+1}, x^{j} - x^{j+1} - g_{des}, \cdots, v^{1} - v^{2}, x^{1} - x^{2} - g_{des}]^{T} \tag{7}$$
$$\boldsymbol{u}_{x,n} \stackrel{\text{def}}{=} [a^{n}, \cdots, a^{j}, \cdots, a^{1}]^{T} \tag{8}$$
$$\boldsymbol{\xi}_{y,n} \stackrel{\text{def}}{=} \left[e_{\varphi}^{n}, y^{n} - y_{des}^{n}, \cdots, e_{\varphi}^{j}, y^{j} - y_{des}^{j}, \cdots, e_{\varphi}^{1}, y^{1} - y_{des}^{1}\right]^{T} \tag{9}$$
$$\boldsymbol{u}_{y,n} \stackrel{\text{def}}{=} \left[\delta_{f}^{n}, \cdots, \delta_{f}^{j}, \cdots, \delta_{f}^{1}\right]^{T} \tag{10}$$

where j is the index of CAVs in a CACC platoon.

B. System Dynamics

The dynamics of the CACC system is modeled in Theorem 1 based on a nonlinear bicycle model [23]. An assumption is adopted for the formulation as follows:

Assumption 2: Vehicle slip angle β, front wheel angle δ_f, and heading angle φ are small. Therefore, $\cos(e_{\varphi} + \beta) \approx 1$, $\sin(e_{\varphi} + \beta) \approx e_{\varphi}$, $\tan\beta \approx \sin\beta$, $\sin\delta_f \approx \delta_f$, $\cos\delta_f \approx 1$, and $cos(e_{\varphi}) \approx 1$.

Theorem 1: Vehicle dynamics is described as follows:

$$f_x(\boldsymbol{\xi}_{x,n}, \boldsymbol{u}_{x,n}, t) = \frac{d\boldsymbol{\xi}_{x,n}}{dt} = \boldsymbol{A}_{x,n}\boldsymbol{\xi}_{x,n} + \boldsymbol{B}_{x,n}\boldsymbol{u}_{x,n} + \boldsymbol{C}_{x,n}a^{\alpha} \tag{11}$$
$$f_y(\boldsymbol{\xi}_{y,n}, \boldsymbol{u}_{y,n}, t) = \frac{d\boldsymbol{\xi}_{y,n}}{dt} = \boldsymbol{A}_{y,n}\boldsymbol{\xi}_{y,n} + \boldsymbol{B}_{y,n}\boldsymbol{u}_{y,n} + \boldsymbol{C}_{y,n} \tag{12}$$
$$\boldsymbol{A}_{x,n} \stackrel{\text{def}}{=} \begin{bmatrix} 0 & 0 & & & \\ 1 & 0 & & & \\ & \ddots & & & \\ & & 0 & 0 & \\ & & 1 & 0 & \end{bmatrix}_{2n\times 2n} \tag{13}$$
$$\boldsymbol{B}_{x,n} \stackrel{\text{def}}{=} \begin{bmatrix} 1 & & & \\ 0 & & & \\ -1 & 1 & & \\ & 0 & & \\ & -1 & \ddots & \\ & & & 1 \\ & & & 0 \end{bmatrix}_{2n\times 2n} \tag{14}$$
$$\boldsymbol{C}_{x,n} \stackrel{\text{def}}{=} [-1, 0 \cdots, 0]_{2n}^{T} \tag{15}$$
$$\boldsymbol{A}_{y,n} \stackrel{\text{def}}{=} \begin{bmatrix} 0 & 0 & & & \\ v & 0 & & & \\ & \ddots & & & \\ & & 0 & 0 & \\ & & v & 0 & \end{bmatrix}_{2n\times 2n} \tag{16}$$
$$\boldsymbol{B}_{y,n} \stackrel{\text{def}}{=} \begin{bmatrix} \frac{v}{l_{fr}} & & & \\ 0 & & & \\ & \ddots & & \\ & & \frac{v}{l_{fr}} & \\ & & 0 & \end{bmatrix}_{2n\times 2n} \tag{17}$$
$$\boldsymbol{C}_{y,n} \stackrel{\text{def}}{=} v\kappa[-1, 0, -1, 0 \cdots, -1, 0]_{2n}^{T} \tag{18}$$

Proof:

The conventional nonlinear bicycle model is formulated as follows [24]:

$$\frac{dx}{dt} = v\cos(e_{\varphi} + \beta) \tag{19}$$
$$\frac{dy}{dt} = v\sin(e_{\varphi} + \beta) \tag{20}$$
$$\frac{de_{\varphi}}{dt} = \frac{v}{l_r}\sin\beta - v\cos(e_{\varphi} + \beta)\kappa \tag{21}$$
$$\frac{dv}{dt} = a \tag{22}$$
$$\beta = \tan^{-1}\left(\frac{l_r}{l_{fr}}\tan\delta_f\right) \tag{23}$$

By applying Assumption 2, equations (19), (20), (21), (22), and (23) are linearized for solving convenience as follows:

$$\frac{dx}{dt} = v \tag{24}$$
$$\frac{dv}{dt} = a \tag{25}$$
$$\frac{dy}{dt} = ve_{\varphi} \tag{26}$$
$$\frac{de_{\varphi}}{dt} = v\left(\frac{\delta_f}{l_{fr}} - \kappa\right) \tag{27}$$

Based on equations (24), (25), (26), and (27), equations (11) and (12) are derived. This concludes the proof. ■

C. Cost Function

Longitudinal and lateral cost functions are formulated into a quadratic form as follows:

$$J_x = \int_0^T L_x\, dt + M_x \tag{28}$$
$$J_y = \int_0^T L_y\, dt + M_y \tag{29}$$
$$L_x = \frac{1}{2}\boldsymbol{\xi}_{x,n}^{T}\boldsymbol{Q}_{x,n}\boldsymbol{\xi}_{x,n} + \frac{1}{2}\boldsymbol{u}_{x,n}^{T}\boldsymbol{R}_{x,n}\boldsymbol{u}_{x,n} \tag{30}$$
$$L_y = \frac{1}{2}\boldsymbol{\xi}_{y,n}^{T}\boldsymbol{Q}_{y,n}\boldsymbol{\xi}_{y,n} + \frac{1}{2}\boldsymbol{u}_{y,n}^{T}\boldsymbol{R}_{y,n}\boldsymbol{u}_{y,n} \tag{31}$$
$$M_x = 0 \tag{32}$$
$$M_y = 0 \tag{33}$$
$$\boldsymbol{Q}_{x,n} \stackrel{\text{def}}{=} \begin{bmatrix} q_v & & & & \\ & q_g & & & \\ & & \ddots & & \\ & & & q_v & \\ & & & & q_g \end{bmatrix}_{2n\times 2n} \tag{34}$$
$$\boldsymbol{R}_{x,n} \stackrel{\text{def}}{=} r_a\boldsymbol{I}_{n\times n} \tag{35}$$
$$\boldsymbol{Q}_{y,n} \stackrel{\text{def}}{=} \begin{bmatrix} q_{\varphi} & & & & \\ & q_y & & & \\ & & \ddots & & \\ & & & q_{\varphi} & \\ & & & & q_y \end{bmatrix}_{2n\times 2n} \tag{36}$$
$$\boldsymbol{R}_{y,n} \stackrel{\text{def}}{=} r_{\delta}\boldsymbol{I}_{n\times n} \tag{37}$$

Manuscript 497 submitted to 2021 32nd IEEE Intelligent Vehicles Symposium (IV).
Received April 7, 2021.

where J is the total cost; L is the running cost; M is the terminal cost; $\boldsymbol{Q}_{x,n}$, $\boldsymbol{R}_{x,n}$ $\boldsymbol{Q}_{y,n}$, and $\boldsymbol{R}_{y,n}$ are all non-negative weighting factors. The running cost L consists of state error cost and control cost to make a balance between the running objective and control efforts. The terminal cost M is set to zero to ensure that the terminal state meets with the objective.

D. Constraints

The proposed controller is bounded by collision avoidance, desired speed range, geometry boundaries, acceleration capability, and yaw angle constraints.

Inner-platoon collision avoidance is realized by regulating the gap in a platoon as follows:

$$x^j - x^{j+1} > g_{min} \tag{38}$$

where g_{min} is the safe following gap in a CACC platoon.

Outer-platoon collision avoidance is ensured by front collision avoidance and rear collision avoidance as follows:

$$x^f - x^1 > g_{min}^{HV} \tag{39}$$

$$x^n - x^r > g_{min}^{HV} \tag{40}$$

where g_{min}^{HV} is the safe following gap between a CAV and a HV.

Vehicles should travel within road geometry boundaries:

$$y_{min} \le y \le y_{max} \tag{41}$$

Vehicle's acceleration should be bounded by vehicle capability and comfort:

$$a_{min} \le a \le a_{max} \tag{42}$$

Vehicle's front wheel angle should be within its steering range:

$$\delta_{f\,min} \le \delta_f \le \delta_{f\,max} \tag{43}$$

E. Solution Algorithm

A solution algorithm previously developed by this research group is borrowed [25]. It is further enhanced here to be better compatible with the problem of interest, as illustrated in Table II. It can accelerate computation speed greatly by predetermining the optimal terminal state. In each iteration cycle, this algorithm involves a backward calculation of concomitant matrices and a forward calculation of control vector and state vector.

By applying the Euler Method, the formulated controllers are discretized into N steps with the time step length τ. The following algorithm can be adopted.

TABLE II SOLUTION ALGORITHM

Input: initial state $\boldsymbol{\xi}_0$, $\boldsymbol{Q}$, $\boldsymbol{R}$, number of control steps N
Output: optimal control $\boldsymbol{u}_i$ and state $\boldsymbol{\xi}_i$ for each step

1. Calculate $\boldsymbol{A}_i$, $\boldsymbol{B}_i$, and $\boldsymbol{C}_i$ for $i \in \{0,1,\cdots,N\}$

$$\boldsymbol{A}_i = \tau\boldsymbol{A} + \boldsymbol{I} \tag{44}$$

$$\boldsymbol{B}_i = \tau\boldsymbol{B} \tag{45}$$

$$\boldsymbol{C}_i = \tau\boldsymbol{C}a_{des} \tag{46}$$

2. For terminal step $i = N+1$:

$$\widetilde{\boldsymbol{Q}}_{N+1} \stackrel{\text{def}}{=} \boldsymbol{Q} \tag{47}$$

$$\widetilde{\boldsymbol{D}}_{N+1} \stackrel{\text{def}}{=} \boldsymbol{0} \tag{48}$$

3. For $i \in \{N, N-1, \cdots, 1\}$, calculate concomitant matrices backward:

$$\boldsymbol{D}_i = -\boldsymbol{Q}\boldsymbol{\xi}_{des\,i} \tag{49}$$

$$\widetilde{\boldsymbol{Q}}_i = \boldsymbol{Z}_{2_i}^T\boldsymbol{R}_i\boldsymbol{Z}_{2_i} + \boldsymbol{Z}_{4_i}^T\widetilde{\boldsymbol{Q}}_{i+1}\boldsymbol{Z}_{4_i} + \boldsymbol{Q}_i \tag{50}$$

$$\widetilde{\boldsymbol{D}}_i = \boldsymbol{Z}_{2_i}^T\boldsymbol{R}_i\boldsymbol{Z}_{3_i} + \boldsymbol{Z}_{4_i}^T\widetilde{\boldsymbol{Q}}_{i+1}\boldsymbol{Z}_{5_i} + \boldsymbol{Z}_{4_i}^T\widetilde{\boldsymbol{D}}_{i+1} + \boldsymbol{D}_i \tag{51}$$

with

$$\boldsymbol{Z}_{1_i} = (\boldsymbol{R}_i + \boldsymbol{B}_i^T\widetilde{\boldsymbol{Q}}_{i+1}\boldsymbol{B}_i)^{-1} \tag{52}$$

$$\boldsymbol{Z}_{2_i} = -\boldsymbol{Z}_{1_i}\boldsymbol{B}_i^T\widetilde{\boldsymbol{Q}}_{i+1}\boldsymbol{A}_i \tag{53}$$

$$\boldsymbol{Z}_{3_i} = -\boldsymbol{Z}_{1_i}\boldsymbol{B}_i^T\left(\widetilde{\boldsymbol{Q}}_{i+1}\boldsymbol{C}_i + \widetilde{\boldsymbol{D}}_{i+1}\right) \tag{54}$$

$$\boldsymbol{Z}_{4_i} = \boldsymbol{A}_i + \boldsymbol{B}_i\boldsymbol{Z}_{2_i} \tag{55}$$

$$\boldsymbol{Z}_{5_i} = \boldsymbol{B}_i\boldsymbol{Z}_{3_i} + \boldsymbol{C}_i \tag{56}$$

4. For $i \in \{0,1,\cdots,N\}$, calculate control vector and state vector forward:

$$\boldsymbol{u}_i = \boldsymbol{Z}_{2_i}\boldsymbol{\xi}_i + \boldsymbol{Z}_{3_i} \tag{57}$$

$$\boldsymbol{\xi}_{i+1} = \boldsymbol{Z}_{4_i}\boldsymbol{\xi}_i + \boldsymbol{Z}_{5_i} \tag{58}$$

IV. STRING STABILITY ANALYSIS

String stability is analyzed in this section. Concerned with string stability, the control law of the proposed longitudinal controller is first demonstrated.

A. Control Law

The control law is formulated in Theorem 2. The Pontryagin's Minimum Principle (PMP) method is adopted to compute the optimal solution. It is defined as follows:

Definition 2 (PMP): The necessary conditions for the optimal solution $\boldsymbol{u}_x^*$ are as follows:

$$H(\boldsymbol{\xi}_{x,n}, \boldsymbol{u}_{x,n}, \boldsymbol{\lambda}_n, t) \stackrel{\text{def}}{=} L_x(\boldsymbol{\xi}_{x,n}, \boldsymbol{u}_{x,n}, t) + \boldsymbol{\lambda}_{x,n}^T f_x(\boldsymbol{\xi}_{x,n}, \boldsymbol{u}_{x,n}, t) \tag{59}$$

$$H\left(\boldsymbol{\xi}_{x,n}^*, \boldsymbol{u}_{x,n}^*, \boldsymbol{\lambda}_n^*, t\right) \le H\left(\boldsymbol{\xi}_{x,n}, \boldsymbol{u}_{x,n}, \boldsymbol{\lambda}_n, t\right) \tag{60}$$

$$M_x\left(\boldsymbol{\xi}_{x,n}, t\right) + H\left(\boldsymbol{\xi}_{x,n}, \boldsymbol{u}_{x,n}, \boldsymbol{\lambda}_n, t\right) = \boldsymbol{0} \tag{61}$$

$$-\frac{d\boldsymbol{\lambda}}{dt} = \frac{\partial H}{\partial \boldsymbol{\xi}_{x,n}} = \frac{\partial f}{\partial \boldsymbol{\xi}_{x,n}}\boldsymbol{\lambda}_n + \frac{\partial L}{\partial \boldsymbol{\xi}_{x,n}} \tag{62}$$

$$\boldsymbol{\lambda}_n(t) = \frac{\partial M_{x,n}(\boldsymbol{\xi}_{x,n}, t)}{\partial \boldsymbol{\xi}_{x,n}(t)} \tag{63}$$

where $\boldsymbol{\lambda}$ is a co-state vector in the Hamiltonian function H.

Theorem 2: The control law of the proposed longitudinal controller is as follows:

$$\boldsymbol{u}_{x,n}^* = -\boldsymbol{R}_{x,n}^{-1}\boldsymbol{B}_{x,n}^T\boldsymbol{\lambda}_n \tag{64}$$

$$-\frac{d\boldsymbol{\lambda}_n}{dt} = \boldsymbol{Q}_{x,n}\boldsymbol{\xi}_{x,n} + \boldsymbol{A}_{x,n}^T\boldsymbol{\lambda}_n \tag{65}$$

Proof:

For a quadratic optimization problem, optimal solution is where the extreme value is. Therefore, equation (60) indicates:

$$\frac{\partial H}{\partial \boldsymbol{u}_{x,n}^*} = \boldsymbol{0} \tag{66}$$

By substituting equations (11), (30), and (59) into equation (66), equation (64) is derived. By substituting equations (11) and (30) into equation (62), equation (65) is derived. It concludes the proof. ■

B. String Stability Proof

Based on the proposed backward-looking information topology, all CAVs in a platoon are maneuvered to minimize the gap error between any CAV and its rear vehicle. Therefore, string stability criterion is defined in Definition 3 by adopting existing string stability definitions [17, 26, 27].

Definition 3: Considering a platoon with $n \in \mathbb{N}$ CAVs, the platoon is string stable if and only if:

$$\left\|\Theta_{n,j,j+1}\right\|_2 \stackrel{\text{def}}{=} \frac{\|a^j(s)\|_2}{\|a^{j+1}(s)\|_2} \le 1,\ \forall j \in [1,n] \tag{67}$$

where $\Theta_{n,j,j+1}$ is the acceleration oscillation transfer function between the jth vehicle and its rear vehicle $j+1$; $\|\cdot\|_2$ denotes

2-norm; $a^j(s)$ is the acceleration oscillation in frequency domain.

To transform functions and variables from time domain to frequency domain, the Laplace transform is adopted as follows:

Definition 4 (Laplace transform): Function $g(t)$ with $t \geq 0$ can be transformed into frequency domain as follows:

$$G(s) = \mathcal{L}\{g(t)\} = \int_0^\infty g(t)e^{-st}dt \tag{68}$$

$$s \triangleq \iota\omega \ (\omega \in \mathbb{R}^+) \tag{69}$$

where e denotes the natural logarithm; ι denotes imaginary number; ω denotes angular speed in Laplace domain.

Following three lemmas are proposed for string stability proof. Lemma 1 formulates the transfer function between the jth CAV and the virtual vehicle. Lemma 2 formulates the recursive expression of $\Theta_{n,n,\alpha}$. Lemma 3 formulates the recursive expression of $\Theta_{n,j,j+1}$.

Lemma 1: Transfer function between the jth CAV and the virtual vehicle is as follows:

$$\Theta_{n,j,\alpha} = \boldsymbol{O}_{n,j}\left(\boldsymbol{R}_{x,n} - \boldsymbol{M}_n\boldsymbol{B}_{x,n}\right)^{-1}\boldsymbol{M}_n\boldsymbol{C}_{x,n} \tag{70}$$

where

$$\boldsymbol{O}_{n,j} \triangleq \left[\underbrace{0\cdots 0}_{n-j}\ 1, \underbrace{0\cdots 0}_{j-1}\right]_{1\times n} \tag{71}$$

$$\boldsymbol{E}_n \triangleq \left(s\boldsymbol{I} + \boldsymbol{A}_{x,n}^T\right)^{-1} \tag{72}$$

$$\boldsymbol{F}_n \triangleq \left(s\boldsymbol{I} - \boldsymbol{A}_{x,n}\right)^{-1} \tag{73}$$

$$\boldsymbol{M}_n \triangleq \boldsymbol{B}_{x,n}^T\boldsymbol{E}_n\boldsymbol{Q}_{x,n}\boldsymbol{F}_n \tag{74}$$

Proof:

By applying Definition 4, state vector, control vector, and co-state vector are transformed into frequency domain as follows:

$$\boldsymbol{\mathcal{X}}_n(s) \triangleq \mathcal{L}\{\boldsymbol{\xi}_{x,n}(t)\} \tag{75}$$

$$\boldsymbol{\mathcal{U}}_n(s) \triangleq \mathcal{L}\{\boldsymbol{u}_{x,n}(t)\} \tag{76}$$

$$\boldsymbol{\mathcal{r}}_n(s) \triangleq \mathcal{L}\{\boldsymbol{\lambda}_n(t)\} \tag{77}$$

By applying Definition 4, equations (11), (64), and (65) are transformed into frequency domain as follows:

$$\boldsymbol{\mathcal{X}}_n = \left(s\boldsymbol{I} - \boldsymbol{A}_{x,n}\right)^{-1}\left(\boldsymbol{B}_{x,n}\boldsymbol{\mathcal{U}}_n + \boldsymbol{C}_{x,n}a^\alpha(s)\right) \tag{78}$$

$$\boldsymbol{\mathcal{U}}_n = -\boldsymbol{R}_{x,n}^{-1\ -1}\boldsymbol{B}_{x,n}^T\boldsymbol{\mathcal{r}}_n \tag{79}$$

$$\boldsymbol{\mathcal{r}}_n = -\left(s\boldsymbol{I} + \boldsymbol{A}_{x,n}^T\right)^{-1}\boldsymbol{Q}_{x,n}\boldsymbol{\mathcal{X}}_n \tag{80}$$

Substituting equation (78) and (80) into equation (79):

$$\boldsymbol{\mathcal{U}}_n = \left(\boldsymbol{R}_{x,n} - \boldsymbol{M}_n\boldsymbol{B}_{x,n}\right)^{-1}\boldsymbol{M}_n\boldsymbol{C}_{x,n}a^\alpha(s) \tag{81}$$

Based on (67):

$$\Theta_{n,j,\alpha} = \frac{a^j(s)}{a^\alpha(s)} = \frac{\boldsymbol{O}_{n,j}\boldsymbol{\mathcal{U}}_n}{a^\alpha(s)} \tag{82}$$

By substituting equations (71) and (81) into equation (82), equation (70) is derived. This concludes the proof. ■

Lemma 2: The transfer function between the last vehicle and the virtual vehicle is recursive as follows:

$$\Theta_{n+1,n+1,\alpha} = \frac{\boldsymbol{M}_1\boldsymbol{C}_1}{r_a + 2\boldsymbol{M}_1\boldsymbol{C}_1 - \boldsymbol{M}_1\boldsymbol{C}_1\Theta_{n,n,\alpha}} \tag{83}$$

Proof:

The recursive formulation of system dynamics is as follows:

$$f_x\left(\boldsymbol{\xi}_{x,n+1}, \boldsymbol{u}_{x,n+1}, t\right) = \frac{d\boldsymbol{\xi}_{x,n+1}}{dt} = \boldsymbol{A}_{x,n+1}\boldsymbol{\xi}_{x,n+1} + \boldsymbol{B}_{x,n+1}\boldsymbol{u}_{x,n+1} + \boldsymbol{C}_{x,n+1}a^\alpha \tag{84}$$

where

$$\boldsymbol{\xi}_{x,n+1} \triangleq \begin{pmatrix}\boldsymbol{\xi}_{x,1}\\ \boldsymbol{\xi}_{x,n}\end{pmatrix} \tag{85}$$

$$\boldsymbol{u}_{x,n+1} \triangleq \begin{pmatrix}\boldsymbol{u}_{x,1}\\ \boldsymbol{u}_{x,n}\end{pmatrix} \tag{86}$$

$$\boldsymbol{A}_{x,n+1} \triangleq \begin{pmatrix}\boldsymbol{A}_{x,1} & \boldsymbol{0}\\ \boldsymbol{0} & \boldsymbol{A}_{x,n}\end{pmatrix} \tag{87}$$

$$\boldsymbol{B}_{x,n+1} \triangleq \begin{pmatrix}\boldsymbol{B}_{x,1} & \boldsymbol{0}\\ \boldsymbol{C}_{x,n}\boldsymbol{B}_{x,n}\end{pmatrix} \tag{88}$$

$$\boldsymbol{C}_{x,n+1} \triangleq \begin{pmatrix}\boldsymbol{C}_{x,1}\\ \boldsymbol{0}\end{pmatrix} \tag{89}$$

Moreover,

$$\boldsymbol{Q}_{x,n+1} = \begin{pmatrix}\boldsymbol{Q}_{x,1} & \boldsymbol{0}\\ \boldsymbol{0} & \boldsymbol{Q}_{x,n}\end{pmatrix} \tag{90}$$

$$\boldsymbol{R}_{x,n+1} = \begin{pmatrix}r_a^1 & \boldsymbol{0}\\ \boldsymbol{0} & \boldsymbol{R}_{x,n}\end{pmatrix} \tag{91}$$

$$\boldsymbol{O}_{n+1,n+1} = \left(\boldsymbol{O}_{1,1}, \boldsymbol{0}\right) \tag{92}$$

Substituting equations (87), (88), (89), (90), (91), and (92) into equations (71), (72), (73), and (74):

$$\boldsymbol{E}_{n+1} = \begin{pmatrix}\boldsymbol{E}_1 & \boldsymbol{0}\\ \boldsymbol{0} & \boldsymbol{E}_n\end{pmatrix} \tag{93}$$

$$\boldsymbol{F}_{n+1} = \begin{pmatrix}\boldsymbol{F}_1 & \boldsymbol{0}\\ \boldsymbol{0} & \boldsymbol{F}_n\end{pmatrix} \tag{94}$$

$$\boldsymbol{M}_{n+1} = \begin{pmatrix}\boldsymbol{M}_1 & \boldsymbol{C}_{x,n}^T\boldsymbol{E}_n\boldsymbol{Q}_{x,n}\boldsymbol{F}_n\\ \boldsymbol{0} & \boldsymbol{M}_n\end{pmatrix} \tag{95}$$

Applying equations (88), (89), (91), (92), and (95) into equation (70):

$$\boldsymbol{R}_{x,n+1} - \boldsymbol{M}_{n+1}\boldsymbol{B}_{x,n+1} = \begin{pmatrix}r_a - 2\boldsymbol{M}_1\boldsymbol{B}_{x,1} - \boldsymbol{C}_{x,n}^T\boldsymbol{E}_n\boldsymbol{Q}_{x,n}\boldsymbol{F}_n\boldsymbol{B}_{x,n} & \\ -\boldsymbol{M}_n\boldsymbol{C}_{x,n} & \boldsymbol{R}_{x,n} - \boldsymbol{M}_n\boldsymbol{B}_{x,n}\end{pmatrix} \tag{96}$$

$$\left(\boldsymbol{R}_{x,n+1} - \boldsymbol{M}_{n+1}\boldsymbol{B}_{x,n+1}\right)^{-1} = \begin{pmatrix}\left(r_a - 2\boldsymbol{M}_1\boldsymbol{B}_{x,1} + \boldsymbol{M}_1\boldsymbol{B}_{x,1}\Theta_{n,n,\alpha}\right)^{-1} & \\ \left(\boldsymbol{R}_{x,n} - \boldsymbol{M}_n\boldsymbol{B}_{x,n}\right)^{-1}\boldsymbol{M}_n\boldsymbol{C}_{x,n}\left(r_a - 2\boldsymbol{M}_1\boldsymbol{B}_{x,1} + \boldsymbol{M}_1\boldsymbol{B}_{x,1}\Theta_{n,n,\alpha}\right)^{-1} & \end{pmatrix} \tag{97}$$

$$\Theta_{n+1,n+1,\alpha} = \left(\boldsymbol{O}_{1,1}, \boldsymbol{0}\right)\left(\boldsymbol{R}_{x,n+1} - \boldsymbol{M}_{n+1}\boldsymbol{B}_{x,n+1}\right)^{-1}\begin{pmatrix}\boldsymbol{M}_1\boldsymbol{C}_{x,1}\\ \boldsymbol{0}\end{pmatrix} = \boldsymbol{O}_{1,1}\left(r_a - 2\boldsymbol{M}_1\boldsymbol{B}_{x,1} + \boldsymbol{M}_1\boldsymbol{B}_{x,1}\Theta_{n,n,\alpha}\right)^{-1}\boldsymbol{M}_1\boldsymbol{C}_{x,1} \tag{98}$$

Equation (98) concludes the proof. ■

Lemma 3: The transfer function between the CAV j and the CAV $j+1$ is recursive as follows:

$$\Theta_{n+1,j,j+1} = \Theta_{n,j,j+1} \tag{99}$$

Proof:

Based on (85) and (86):

$$\boldsymbol{O}_{n+1,j} = \left(0, \boldsymbol{O}_{n,j}\right) \tag{100}$$

Substituting equations (89), (95), (97), and (100) into equation (70):

$$\Theta_{n+1,j,\alpha} = \boldsymbol{O}_{n,j}\left(\boldsymbol{R}_{x,n} - \boldsymbol{M}_n\boldsymbol{B}_{x,n}\right)^{-1}\boldsymbol{M}_n\boldsymbol{C}_{x,n}\left(r_a - 2\boldsymbol{M}_1\boldsymbol{B}_{x,1} + \boldsymbol{M}_1\boldsymbol{B}_{x,1}\Theta_{n,n,\alpha}\right)^{-1}\boldsymbol{M}_1\boldsymbol{C}_{x,1} = \Theta_{n,j,\alpha}\Theta_{n+1,n+1,\alpha} \tag{101}$$

Then,

$$\frac{\Theta_{n+1,j,\alpha}}{\Theta_{n+1,j+1,\alpha}} = \frac{\Theta_{n,j,\alpha}}{\Theta_{n,j+1,\alpha}} \tag{102}$$

Equation (102) indicate equation (99). ■

Theorem 3: The proposed controller is proven with string stability.

Proof:

For a platoon with $n = 1$, the transfer function is as follows:

$$\Theta_{1,1,\alpha} = \frac{q_g - q_v s^2}{q_g - q_v s^2 + r_a s^4} \quad (103)$$

Since $s^2 < 0$, $s^4 > 0$, $q_v, q_g, r_a > 0$,

$$0 < \Theta_{1,1,\alpha} < 1 \quad (104)$$

Since $r_a > 0$, following inequality is derived by substituting equation (103) into equation (83):

$$0 < \Theta_{n,n,\alpha} < 1 \quad (105)$$

Based on equation (99):

$$\Theta_{n+1,j,j+1} = \Theta_{n,j,j+1} = \cdots = \Theta_{j,j,\alpha} \quad (106)$$

Based on equations (105) and (106):

$$0 < \Theta_{n,j,j+1} < 1 \quad (107)$$

It confirms the string stability criterion in Definition 3. This concludes the proof. ■

V. Evaluation

The proposed CACCLC controller is evaluated from the following aspects: i) making space to change lane function validation; ii) platoon string stability. The evaluation is conducted on a joint simulation platform consisting of PreScan and Matlab/Simulink.

A. Experiment Design

Following settings are adopted for the evaluation.

- Desired space gap: 10m (3.28ft);
- Acceleration range: $[-5,3]\mathrm{m/s^2}$;
- Steering angle range: $[-450°, 450°]$;
- Lane width: 3m (9.84ft).

B. Test Scenario

The evaluation scenario is illustrated in Figure 4. It is a typical scenario that a CACC platoon would encounter. In this scenario, a CACC platoon is impeded by the surrounding traffic. In order to drive to the ramp, the CACC platoon has to maneuver through the gap. The CACC platoon is a vehicle string consisting of five vehicles. The proposed CACCLC controller is adopted.

Two road types have been tested:

- Arterial: a road segment with a speed limit of 72 km/h (45 mph);
- Freeway: a road segment with a speed limit of 105 km/h (65 mph).

In order to evaluate the stability of the proposed controller, speed perturbation is introduced as shown in Figure 5. $\pm 7.2 km/h$ is conducted on the desired speed of the last CAV.

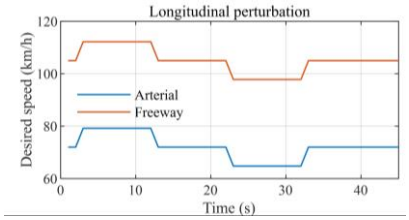

Figure 5. Speed pertrubation

C. Measurements of Effectiveness

The making space to change lane function is verified by vehicle trajectory plots. String stability is verified by utilizing the following Measurements of Effectiveness (MOE): mean of absolute gap error: $\bar{e}_g$.

D. Results

Results confirm that the proposed controller is: i) capable of making space to change lane successfully; ii) with string stability; iii) with 15 milliseconds average computation time on a laptop equipped with an Intel i7-8750H CPU.

Figure 6 verify that the proposed controller functions as promised. It is able to make space for a CACC platoon to change lane by utilizing a small gap. Figure 6 illustrates the trajectory of a CACC lane change process on arterial and freeway. Performance of the proposed controller on both arterial and freeway are demonstrated. As shown in the figures, all CAVs are able to successfully make the lane-change and maintaining the form of platoon. No collision occurs in the CACC lane change process.

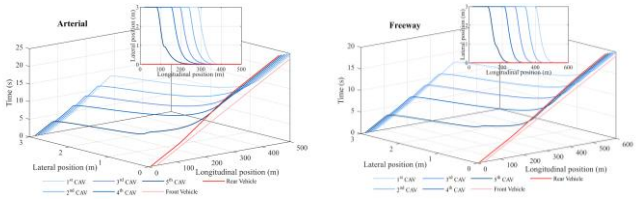

Figure 6. Vehicle trajectory

The string stability of the proposed controller is confirmed. Figure 7 illustrates the acceleration trajectory of the platoon. Figure 8 illustrates the gap error trajectory of the platoon. The three figures demonstrate that acceleration and gap error trajectories of front CAVs have lower peaks compared to the rear CAVs. Acceleration and gap error oscillation lowers along the BL information topology from the last CAV to the first CAV. Figure 9 illustrates the MOE (mean of absolute gap error $\bar{e}_g$) in a CACC platoon. $\bar{e}_g$ decreases about 66.67% along the BL information topology. Specifically, $\bar{e}_g$ decreases from 0.8 meters to 0.31 meters on arterial and from 0.94 meters to 0.26 meters on freeway. It demonstrates that the proposed CACCLC controller is with string stability.

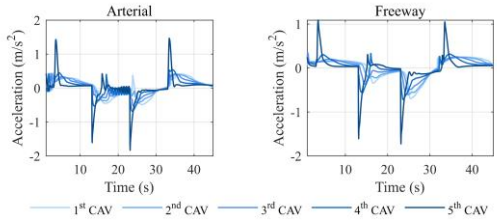

Manuscript 497 submitted to 2021 32nd IEEE Intelligent Vehicles Symposium (IV).
Received April 7, 2021.

Figure 7. Acceleration trajectory

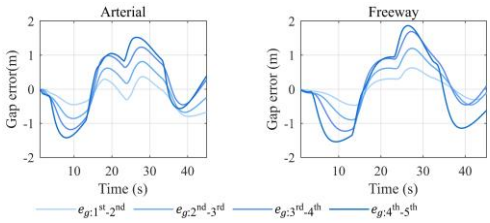

Figure 8. Gap error trajectory

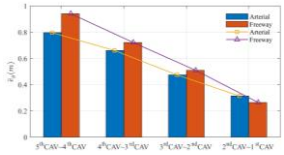

Figure 9. Mean of absolute gap error in a CACC platoon

VI. Conclusion and Future Research

This research proposes a CACCLC controller. It is designed for making space to change lane successfully. The proposed controller has the following features: i) capable of making space to change lane by adopting a new Backward-Looking information topology; ii) with string stability; iii) with consideration of vehicle dynamics. The proposed CACCLC controller is evaluated on a joint simulation platform consisting of PreScan and Matlab/Simulink. Results demonstrate that:

- Computation time of the proposed CACCLC controller is approximately 15 milliseconds when running on a laptop equipped with an Intel i7-8750H CPU. This indicates that the proposed controller is ready for real-time implementation
- The proposed CACCLC controller functions as expected and is capable of making space to change lane by utilizing small lane-change gap for single vehicle.
- The proposed CACCLC controller is confirmed with string stability. 66.67% gap error is eliminated from the end to the start of the platoon.

In this research, the communication delay is not accommodated. Future research could enhance the controller accordingly.

References

[1] S. E. Shladover, C. Nowakowski, J. O'Connell, and D. Cody, "Cooperative adaptive cruise control: Driver selection of car-following gaps," in *17th ITS World CongressITS JapanITS AmericaERTICO*, 2010.

[2] C. Nowakowski, J. O'Connell, S. E. Shladover, and D. Cody, "Cooperative adaptive cruise control: Driver acceptance of following gap settings less than one second," in *Proceedings of the Human Factors and Ergonomics Society Annual Meeting*, 2010, vol. 54, no. 24, pp. 2033-2037: SAGE Publications Sage CA: Los Angeles, CA.

[3] S. E. Shladover, D. Su, and X.-Y. Lu, "Impacts of cooperative adaptive cruise control on freeway traffic flow," *Transportation Research Record,* vol. 2324, no. 1, pp. 63-70, 2012.

[4] M. Zhou, X. Qu, and S. Jin, "On the impact of cooperative autonomous vehicles in improving freeway merging: a modified intelligent driver model-based approach," *IEEE Transactions on Intelligent Transportation Systems,* vol. 18, no. 6, pp. 1422-1428, 2017.

[5] J. B. Rawlings and D. Q. Mayne, "Model predictive control: Theory and design," 2009.

[6] I. G. Jin and G. Orosz, "Connected cruise control among human-driven vehicles: Experiment-based parameter estimation and optimal control design," *Transportation Research Part C: Emerging Technologies,* vol. 95, pp. 445-459, 2018.

[7] J. Hu, H. Wang, X. Li, and X. Li, "Modelling merging behaviour joining a cooperative adaptive cruise control platoon," *IET Intelligent Transport Systems,* 2020.

[8] B. Van Arem, C. J. Van Driel, and R. Visser, "The impact of cooperative adaptive cruise control on traffic-flow characteristics," *IEEE Transactions on Intelligent Transportation Systems,* vol. 7, no. 4, pp. 429-436, 2006.

[9] A. Vahidi and A. Sciarretta, "Energy saving potentials of connected and automated vehicles," *Transportation Research Part C: Emerging Technologies,* 2018.

[10] B. B. Park, K. Malakorn, and J. Lee, "Quantifying Benefits of Cooperative Adaptive Cruise Control Towards Sustainable Transportation System," 2011.

[11] H. Liu, W. Zhuang, G. Yin, Z. Tang, and L. Xu, "Strategy for heterogeneous vehicular platoons merging in automated highway system," in *2018 Chinese Control And Decision Conference (CCDC)*, 2018, pp. 2736-2740: IEEE.

[12] H. H. Bengtsson, L. Chen, A. Voronov, and C. Englund, "Interaction protocol for highway platoon merge," in *2015 IEEE 18th International Conference on Intelligent Transportation Systems*, 2015, pp. 1971-1976: IEEE.

[13] C. Toy, K. Leung, L. Alvarez, and R. Horowitz, "Emergency vehicle maneuvers and control laws for automated highway systems," *IEEE Transactions on Intelligent Transportation Systems,* vol. 3, no. 2, pp. 109-119, 2002.

[14] H. C.-H. Hsu and A. Liu, "Kinematic design for platoon-lane-change maneuvers," *IEEE Transactions on Intelligent Transportation Systems,* vol. 9, no. 1, pp. 185-190, 2008.

[15] X. Liu, G. Zhao, N. Masoud, and Q. Zhu, "Trajectory Planning for Connected and Automated Vehicles: Cruising, Lane Changing, and Platooning," 2020.

[16] Z. Huang, D. Chu, C. Wu, and Y. He, "Path Planning and Cooperative Control for Automated Vehicle Platoon Using Hybrid Automata," *IEEE Transactions on Intelligent Transportation Systems,* vol. 20, no. 3, pp. 959-974, 2018.

[17] J. Ploeg, B. T. Scheepers, E. Van Nunen, N. Van de Wouw, and H. Nijmeijer, "Design and experimental evaluation of cooperative adaptive cruise control," in *2011 14th International IEEE Conference on Intelligent Transportation Systems (ITSC)*, 2011, pp. 260-265: IEEE.

[18] G. J. Naus, R. P. Vugts, J. Ploeg, M. J. van de Molengraft, and M. Steinbuch, "String-stable CACC design and experimental validation: A frequency-domain approach," *IEEE Transactions on vehicular technology,* vol. 59, no. 9, pp. 4268-4279, 2010.

[19] J. Zhang, X. Jia, and Z. Zhou, "A pre-compensation control algorithm for vehicle platoon stability problem," *Optik-International Journal for Light and Electron Optics,* vol. 126, no. 19, pp. 2208-2213, 2015.

[20] E. Shaw and J. K. Hedrick, "String stability analysis for heterogeneous vehicle strings," in *American Control Conference, 2007. ACC'07*, 2007, pp. 3118-3125: IEEE.

[21] V. Milanés, S. E. Shladover, J. Spring, C. Nowakowski, H. Kawazoe, and M. Nakamura, "Cooperative adaptive cruise control in real traffic situations," *IEEE Transactions on Intelligent Transportation Systems,* vol. 15, no. 1, pp. 296-305, 2014.

[22] A. Ghasemi, R. Kazemi, and S. Azadi, "Stable decentralized control of a platoon of vehicles with heterogeneous information feedback," *IEEE Transactions on Vehicular Technology,* vol. 62, no. 9, pp. 4299-4308, 2013.

[23] R. Rajamani, *Vehicle dynamics and control*. Springer Science & Business Media, 2011.

[24] H. Wang, X. Li, Y. Zhang, B. Sun, W. Ma, and J. Hu, "Motion Planning Algorithm Under Partially Connected and Automated Environment," 2019.

[25] Y. B. Yu Zhang, Meng Wang, Jia Hu, "Chang-Hu's Optimal Motion Planning Framework for Cooperative Automation: Mathematical Formulation, Solution, and Applications," *Transportation Research Board Annual Meeting,* 2020.

[26] J. Ploeg, N. Van De Wouw, and H. Nijmeijer, "Lp string stability of cascaded systems: Application to vehicle platooning," *IEEE Transactions on Control Systems Technology,* vol. 22, no. 2, pp. 786-793, 2013.

[27] Y. Bail, Y. Zhang, M. Wang, and J. Hu, "Optimal control based CACC: Problem formulation, solution, and stability analysis," in *2019 IEEE Intelligent Vehicles Symposium (IV)*, 2019, pp. 7-7: IEEE.

Manuscript 497 submitted to 2021 32nd IEEE Intelligent Vehicles Symposium (IV).
Received April 7, 2021.